A Three-Dimension Double-Population Thermal Lattice BGK Model for Simulation of Natural Convection Heat Transfer in a Cubic Cavity

*C. S. NOR AZWADI and S. SYAHRULLAIL
Department of Thermo-fluid
Universiti Teknologi Malaysia
81310 UTM Skudai, Johor
MALAYSIA
azwadi@fkm.utm.my http://www.fkm.utm.my/~azwadi

Abstract: - In this paper, a double-population thermal lattice Boltzmann was applied to solve three dimensional, incompressible, thermal fluid flow problem. The simplest lattice BGK D3Q6 model was proposed to determine the temperature field while D3Q15 or D3Q19 for the density and velocity fields. The simulation of natural convection in a cubic cavity with Prandtl number 0.71 and Rayleigh number ranging from 10^3 to 10^5 were carried out and compared with the published results in literature. It was observed that the combination of D3Q6 and D3Q19 produces better numerical stability and accuracy compared to D3Q6 with D3Q15 for the simulation at high Rayleigh numbers.

Key-Words: - Double population, lattice Boltzmann, distribution function, BGK collision, natural convection

1 Introduction

For more than a decade, lattice Boltzmann method (LBM) has been demonstrated to be a very effective numerical tool for a broad variety of complex fluid flow phenomena that are problematic for conventional methods [1]. Although as a new comer in numerical scheme, the LBM has found recent successes in the host of fluid dynamical problems including flow in porous media [2], magnetohydrodynamics [3], acoustic [4], turbulence [5], and many others [6][7][8]. Compared with traditional computational fluid dynamics, LBM algorithms are much easier to be implemented especially in complex geometries [9] and multicomponent flows [10].

Historically, LBM was derived from lattice gas automata (LGA) [11]. Consequently, LBM inherits some features from it precursor, the LGA method. The first LBM model was a floating-point version of its LGA counterpart. Each particle in LGA model (represented by single bit Boolean integer) was replaced by a single particle distribution function represented by a floating-point number. The lattice structure and the evolution rule remain the same. One important improvement to enhance the computational efficiency has been made for the LBM was that the linearization of collision operator. The uniform lattice structure was remaining unchanged.

The starting point in the lattice Boltzmann scheme is by tracking the evolution of the single-particle distribution function. The concept of particle distribution has already well developed in the field of statistical mechanics while discussing the kinetic theory of gases and liquids. The definition implies the probable number of molecules in a certain volume at a certain time made from a huge number of particles in a system that travel freely, without collision, for distance (mean free path) long compared to their sizes. Once the distribution functions are obtained, the hydrodynamics equations can be derived.

Although LBM approach treats gases and liquids as systems consisting of individual particles, the primary goal of this approach is to build a bridge between the microscopic and macroscopic dynamics, rather than to deal with macroscopic dynamics directly. In other words, the goal is to derive macroscopic equations from microscopic dynamics by means of statistic, rather than to solve macroscopic equations.

The LBM has a number of advantages over other conventional computational fluid dynamics approaches. The algorithm is simple and can be implemented with a kernel of just a few hundred lines. The algorithm can also be easily modified to allow for the application of other, more complex simulation components. For example, the LBM can be extended to describe the evolution of binary mixtures, or extended to allow for more complex boundary conditions. Thus the LBM is an ideal tool in fluid simulation.

Although promising, the current LBM still have few shortcomings that limit its general application as a practical computational fluid dynamics tool. One of these shortcomings, which is specifically addressed in this paper, is lack of reliable thermal lattice Boltzmann model, especially for three-dimensional (3D) system, with low computational cost.

Generally, there are three types of thermal lattice Boltzmann models have been proposed; multi-speed model [12], passive scalar model [13] and double distribution function (DDF) model [14]. The multispeed approach uses the same distribution in defining the macroscopic velocity, pressure and temperature. In addition to mass and momentum, in order to preserve the kinetic energy in the collision on each lattice point, this model requires more variations of speed than those of the isothermal model and equilibrium distribution function usually include higher order velocity terms. However, this model is reported to suffer severe numerical instability, and is not computationally efficient [15].

In the passive scalar model, the flow fields (velocity and density) and the temperature are represented by two different distribution functions. The macroscopic temperature is assumed to satisfy the same evolution equation as a passive scale, which is advected by the flow velocity, but does not affect the flow field. It has been shown that the passive scalar model has better numerical stability than the multi-speed approach [16].

He et al. [14] in their model introduce the internal energy density distribution function, which can be derived from the Boltzmann equation. This model is shown to be a suitable model for simulating real thermal problems. However, the complicated gradient operator term appears in the evolution equation and thus the simplicity property of the lattice Boltzmann scheme has been lost [17][18][19].

Natural convection heat transfer in a square cavity has attracted much attention in recent years due to its wide applications such as cooling of radioactive waste containers, ventilation of rooms, solar energy collectors, crystal growth in liquids, etc. A comprehensive review was presented by Davis [20]. However, among the previous numerical studies pertinent to this problem, little works have been done using 3D simulation model.

As far as authors' knowledge, few attempt have been made to predict the phenomenon of natural convection in a cubic cavity using 3D thermal lattice Boltzmann models. Peng et al. [21] proposed and investigated the efficiency and stability of the DDF model using two different particle velocity models of D3Q15 [22] (three-dimension fifteen-particle velocity) and D3Q19. All macroscopic variables such as density, velocity and temperature fields were calculated using the same models wether D3Q15 or D3Q19. They showed that for the simulation at low Rayliegh number $Ra = 10^3$, the results obtained were almost the same for D3Q15 and D3Q19 models. While for high Rayliegh number simulations $Ra = 10^4$ and 10^5, D3Q19 produced better results than D3Q15 when compared with Navier-Stokes solver. However, both of these models require high computational cost due to the application of high number of particle velocity for both density and temperature distribution functions.

The recent work by Azwadi et al. [23] focused on the development of the lattice model for the calculation of temperature field. They found that an eight-particle velocity model, D3Q8 can be developed for the internal energy density distribution function if the viscous and compressive heating effect were neglected. Though Azwadi et al.'s model has been successfully simulated 3D natural convection problem to a certain degree with low computation cost, this model is limited for the simulation at low Rayleigh numbers. They reported that this was due to the limitation on the value of time relaxation for the internal energy density distribution function model where very close to its stability limit at high Rayleigh number simulation. However, for real thermal engineering applications, the value of Rayleigh numbers could achieve up to 10^5. Therefore, a 3D thermal model that is capable in simulating up to this value of Rayleigh number is still demanded.

In this research, works have been done on the improvement of passive scalar model. In passive scalar approach, the distribution function for the temperature field is relatively independent of that for the velocity field, so the passive scalar model can use two independent lattices for two distribution functions respectively. Although Peng and Azwadi et al. have developed lattice models based on DDF approach, however, the final form of governing equations for density and internal energy density were exactly the same as in the passive scalar model if the viscous heat dissipation and the work done by pressure were neglected.

The current investigation is differentiated from previous double-population studies by introducing the simplest passive scalar model of D3Q6 for the calculation of temperature field. The proposed model is then coupled with D3Q15 or D3Q19 for the calculation of density and velocity fields.

The rest of the paper is organized as follow. In the next section, the 3D double-population passive scalar model is constructed. In the sequence section, the proposed model is employed to simulate the natural convection flow in a cubic cavity with two sides walls maintained at different temperature. The final section concludes this study.

2 Double-population Thermal Lattice Boltzmann Model

In 3D lattice Boltzmann method, the physical space is divided into cubic lattices, and the evolution of particle population at each lattice site is computed by using particle distribution function. Following the passive scalar approach proposed by Shan [13] and Guo et al. [24], the evolution of particle distribution functions (discretised in velocity space) are computed by the following equations

$$f_i\left(\mathbf{x}+\mathbf{c}_i\Delta t, t+\Delta t\right)-f_i\left(\mathbf{x},t\right)=\Omega\left(f\right)+F \tag{1}$$

$$g_i\left(\mathbf{x}+\mathbf{c}_i\Delta t, t+\Delta t\right)-g_i\left(\mathbf{x},t\right)=\Omega\left(g\right) \tag{2}$$

where density distribution function $f=f\left(\mathbf{x},t\right)$ is used to calculate density and velocity field and temperature distribution function $g=g\left(\mathbf{x},t\right)$ is used to calculate the temperature field. Both Eqs. (1) and (2) consist of two parts; propagation (left hand side) which refers to the propagation of distribution function to the next node in the direction of its probable velocity, and collision Ω (right hand side) which represent the collision of the particle distribution functions. In lattice Boltzmann formulation, magnitude of $\mathbf{c}$ is set up so that in each time step Δt, every distribution function propagates in a distance of lattice nodes spacing $\Delta\mathbf{x}$. This will ensure that distribution function arrives exactly at the lattice nodes after Δt and collides simultaneously.

Any solution of Eqs. (1) and (2) requires an expression for the collision operator Ω. If the collision is to conserve mass, momentum and energy, it is required that

$$\int\begin{bmatrix}1\\ \mathbf{c}\\ c\end{bmatrix}\Omega\mathrm{d}\mathbf{c}=0 \tag{3}$$

However, the expression for Ω is too complex to be solved [25]. Any replacement of collision must satisfy the conservation law as expressed in Eq. (3). The idea behind this replacement is that large amount of detail of two-body interaction is not likely to influence significantly the values of many experimental measured quantities [26].

There are a few version of collision operator published in the literature. However, the most well accepted version due to its simplicity and efficiency is the Bhatnagar Gross Crook collision model [27] with a single relaxation time. The equation that represents this model is given by

$$\Omega\left(f\right)=-\frac{f_i\left(\mathbf{x},\mathbf{c}_i,t\right)-f_i^{eq}\left(\mathbf{x},\mathbf{c}_i,t\right)}{\tau_f} \tag{4}$$

where f_i^{eq} is the equilibrium distribution function and τ_f is the time to reach equilibrium condition during collision process and is often called the relaxation time. However, the relaxation time of energy carried by the particles to its equilibrium is different to that of momentum. Therefore we need to use a different two relaxation times to characterize the momentum and energy

$$\Omega\left(g\right)=-\frac{g_i\left(\mathbf{x},\mathbf{c}_i,t\right)-g_i^{eq}\left(\mathbf{x},\mathbf{c}_i,t\right)}{\tau_g} \tag{5}$$

Substituting Eqs. (4) and (5) into Eqs. (1) and (2) gives

$$f_i\left(\mathbf{x}+\mathbf{c}_i\Delta t, t+\Delta t\right)-f_i\left(\mathbf{x},t\right)= -\frac{f_i\left(\mathbf{x},\mathbf{c}_i,t\right)-f_i^{eq}\left(\mathbf{x},\mathbf{c}_i,t\right)}{\tau_f}+F \tag{6}$$

$$g_i\left(\mathbf{x}+\mathbf{c}_i\Delta t, t+\Delta t\right)-g_i\left(\mathbf{x},t\right)= -\frac{g_i\left(\mathbf{x},\mathbf{c}_i,t\right)-g_i^{eq}\left(\mathbf{x},\mathbf{c}_i,t\right)}{\tau_g} \tag{7}$$

The macroscopic variables such as density ρ, velocity $\mathbf{u}$, and temperature can be evaluated as the moment to the distribution function

$$\rho=\int f\mathrm{d}\mathbf{c},\ \rho\mathbf{u}=\int \mathbf{c}f\mathrm{d}\mathbf{c},\ \text{and}\ \rho T=\int g\mathrm{d}\mathbf{c} \tag{8}$$

Suffix i in each distribution function indicates the number of microscopic velocity applied to density and temperature distribution function. In the present study, D3Q15 or D3Q19 are used for the density while D3Q6 for the temperature distribution function. The configurations of lattice velocities for density distribution functions are shown in Fig. 1.

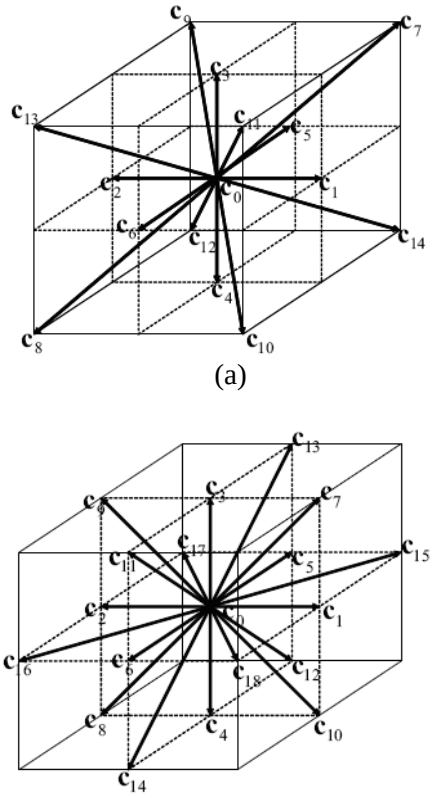

(a)

(b)

Fig. 1 Lattice structure for (a) D3Q15 and (b) D3Q19 models.

The discretised equilibrium distribution function for both D3Q15 and D3Q19 is given as

$$f_i^{eq} = \rho\omega_i\left[1+3\mathbf{c}_i\cdot\mathbf{u}+\frac{9}{2}(\mathbf{c}_i\cdot\mathbf{u})^2-\frac{3}{2}\mathbf{u}^2\right] \tag{9}$$

where $\omega_0 = 2/9$, $\omega_{1-6} = 1/9$ and $\omega_{7-14} = 1/72$ for D3Q15 and $\omega_0 = 1/3$, $\omega_{1-6} = 1/18$ and $\omega_{7-18} = 1/36$ for D3Q19. The time relaxation in both models is related to the fluid viscosity through the same equation as

$$\upsilon = \frac{2\tau_f - 1}{6} \tag{10}$$

We next demonstrate the procedure to non-dimensionalize the lattice Boltzmann equations (Eqs. (6) and (7)). To do this, we define the reference parameters as follow

$$\begin{aligned}&\text{Characteristic length scale, } L\\ &\text{Reference speed, } U\\ &\text{Reference density, } n_{\mathrm{r}}\\ &\text{Time between particle collision, } t_{\mathrm{c}}\end{aligned} \tag{11}$$

The dimensionless lattice Boltzmann equation can be written as

$$\hat{f}_i\left(\hat{\mathbf{x}}+\hat{\mathbf{c}}_i\Delta\hat{t},\hat{t}+\Delta\hat{t}\right)-\hat{f}_i\left(\hat{\mathbf{x}},\hat{t}\right)=-\frac{\hat{f}_i\left(\hat{\mathbf{x}},\hat{t}\right)-\hat{f}_i^{eq}\left(\hat{\mathbf{x}},\hat{t}\right)}{\hat{\tau}_f\varepsilon} \tag{12}$$

where $\hat{\mathbf{c}} = \mathbf{c}/U$, $\hat{\mathbf{x}} = \mathbf{x}/L$, $\hat{t} = tU/L$, $\hat{f} = f/n_r$, $\Delta\hat{t} = \Delta tU/L$ and $\hat{\tau} = \tau/t_c$. The parameter $\varepsilon = t_cU/L$ can be interpreted as either the ratio of collision time to flow time or as the ratio of mean free path to the characteristic length. The same procedure can be applied to obtain the dimensionless form of temperature distribution function. For simplification, all carets will be dropped and any terms referred to later are understood in dimensionless form.

Through a multiscaling, the mass and momentum equations can be derived from the evolution equation of Eq. (1). To see this, we first apply the Taylor series expansion of Eq. (1) and retaining terms up to second order gives

$$\left(\partial_t+\nabla\cdot\mathbf{c}_i\right)f_i+\frac{1}{2}\left(\partial_t^2+2\partial_t\nabla\cdot\mathbf{c}_i+\nabla\nabla:\mathbf{c}_i\mathbf{c}_i\right)f_i \tag{13}$$

In order to relate lattice Boltzmann equation with a macroscopic equation, it is necessary to separate different time scale. This is to indicate different scale of physical phenomena and contribute separately in the final macroscopic equation. To do this, space and time derivation are expanded in terms of Knudsen number ε as follow [28]

$$\partial_t = \varepsilon\partial_{t1}+\varepsilon^2\partial_{t2}+O\left(\varepsilon^3\right) \tag{14}$$

$$\nabla = \varepsilon\nabla+O\left(\varepsilon^2\right) \tag{15}$$

Distribution function f_i is expanded about f_i^{eq} gives

$$f_i = f_i^{eq}+\varepsilon f_i^1+\varepsilon^2 f_i^2+O\left(\varepsilon^3\right) \tag{16}$$

where

$$\sum_i f_i^n = \sum_i \mathbf{c}_i f_i^n = 0 \text{ for } n\geq 1 \tag{17}$$

Eq. (17) implies that the non-equilibrium distribution function f_i^n does not contribute to the local values of density and momentum.

Substituting Eq. (14), (15) and (16) into (13) and regroup the equation to the first order of ε gives

$$\left(\partial_{t1}+\mathbf{c}_i\cdot\nabla\right)f_i^{eq}=-\frac{1}{\tau_f}f_i^1 \tag{18}$$

The equation to order ε^2 is simplified by using Eq. (18) gives

$$\partial_{t2}f_i^{eq}+\left(\partial_{t1}+\mathbf{c}_i\cdot\nabla\right)\left(1-\frac{1}{2\tau_f}\right)f_i^1=-\frac{1}{\tau_f}f_i^2 \tag{19}$$

A summation of Eq. (18) with respect to *i* is taken to give the first order of continuity equation

$$\partial_{t1}\rho+\nabla\left(\rho\mathbf{u}\right)=0 \tag{19}$$

Next, multiplying Eq. (18) by $\mathbf{c}_i$ and taking the summation as above leads to

$$\partial_{t1}\left(\rho\mathbf{u}\right)+\nabla\cdot\prod^{eq}=0 \tag{20}$$

where

$$\prod^{eq}=\sum_i\left(\mathbf{c}_i\mathbf{c}_i\right)f_i \tag{21}$$

is the momentum flux tensor. After some simple mathematics manipulation to satisfy Galilean invariance and isotropic of tensor, the final expression for $\prod^{eq}$ is

$$\prod^{eq}=c_s^2\rho\delta_{\alpha\beta}+\rho u_\alpha u_\beta \tag{22}$$

Substituting Eq. (22) into Eq. (20) results in

$$\partial_{t1}\left(\rho\mathbf{u}\right)+\nabla\cdot\left(\rho\mathbf{u}\mathbf{u}\right)=-\nabla\left(c_s^2\rho\right) \tag{23}$$

Eqs. (19) and (23) are known as Euler equation and the pressure is given by

$$p=c_s^2\rho \tag{24}$$

Similarly, the equation for ρ and $\mathbf{u}$ can be obtained from equation of ε^2. Taking summation with respect to *i* of Eq. (19) gives

$$\partial_{t2}\rho=0 \tag{25}$$

Multiplying Eq. (19) by $\mathbf{c}_i$ and taking the summation as above gives

$$\partial_{t2}\left(\rho\mathbf{u}\right)+\nabla\cdot\left(1-\frac{1}{2\tau_f}\right)\prod^1=0 \tag{26}$$

where

$$\begin{aligned}\prod^1=-\tau_f\Big\{&\left(\frac{1}{3}-c_s^2\right)\partial_\alpha\left(\rho u_\alpha\right)\delta_{\beta\gamma}+\frac{1}{3}\partial_\beta\left(\rho u_\gamma\right)\\&+\frac{1}{3}\partial_\gamma\left(\rho u_\beta\right)-u_\beta\partial_\gamma\left(c_s^2\rho\right)-u_\gamma\partial_\beta\left(c_s^2\rho\right)\\&-\partial_\chi\left(\rho u_\beta u_\gamma u_\chi\right)\Big\}\end{aligned} \tag{27}$$

Combining equations of $O(\varepsilon)$ and $O(\varepsilon^2)$ gives the correct form of the continuity equation

$$\nabla\cdot\mathbf{u}=0 \tag{28}$$

and the momentum equation for an incompressible fluid

$$\partial_t\left(\rho u_\alpha\right)+\partial_\gamma\left(\rho u_\alpha u_\beta\right)=-\partial_\alpha\left(c_s^2\rho\right)+\partial_\beta\left(2\rho\frac{2\tau_f-1}{6}S_{\alpha\beta}\right) \tag{29}$$

where $S_{\alpha\beta}=\frac{1}{2}\left(\partial_\alpha u_\beta+\partial_\beta u_\alpha\right)$, $p=c_s^2\rho$ and the sound speed is given by

$$c_s^2=\frac{1}{3} \tag{30}$$

From above derivations, we can see that the evolution equation of distribution function can lead to the incompressible Navier-Stokes equation through Chapman-Enskog expansion.

It has been proved [29][30] that the effects of heat viscous dissipation and work done by the pressure can be neglected for incompressible flow. Under these assumption, the temperature field is passively advected by the fluid flows and obeys the so-called passive-scalar equation as

$$\frac{\partial T}{\partial t}+\nabla\cdot\left(\mathbf{u}T\right)=\chi\nabla^2T \tag{31}$$

Here, the thermal diffusivity χ can be related to the time relaxation carried by the energy by

$$\chi = \frac{2\tau_g - 1}{6} \tag{32}$$

In current research, the simplest lattice structure of D3Q6 for temperature distribution function is proposed. The configuration of lattice structure is shown in Fig. 2.

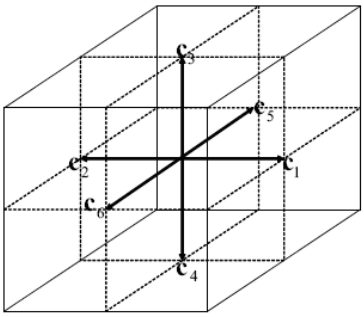

Fig. 2 Lattice structure for D3Q6 model

The corresponding discretised equilibrium distribution function for this lattice model can be written as

$$g_i^{eq} = \frac{1}{6}\rho T\left[1 + 3\mathbf{c}_i \cdot \mathbf{u}\right] \tag{33}$$

Eq. (33) is obtained by assuming that at low Mach number flow, the higher order of $\mathbf{u}^2$ and viscous heat dissipation can be neglected [6]. It also has been proved [23] that the above simplification does not alter the corresponding macroscopic equation of energy. The only change is the value of the constant parameter in the thermal conductivity, which can be absorbed by manipulating the parameter τ_g.

3 Natural Convection in a Cubic Cavity

Numerical simulation for the natural convection in a cubic cavity was carried out to test the validity of the combination of D3Q15 or D3Q19 with D3Q6 thermal lattice Boltzmann model. Fig. 3 shows a schematic diagram of the setup in the simulation.

No-slip boundary condition [11] is imposed on all faces of the cubes. The thermal conditions applied on the left and right walls are $T(x=0,y,z)=T_H$ and $T(x=1,y,z)=T_C$. The other faces being adiabatic, $\partial T/\partial n = 0$ where $\partial T/\partial n$ is the appropriate normal derivative. The temperature difference between the left and right walls introduces a temperature gradient in a fluid, and the consequent density difference induces a fluid motion, that is, convection [31].

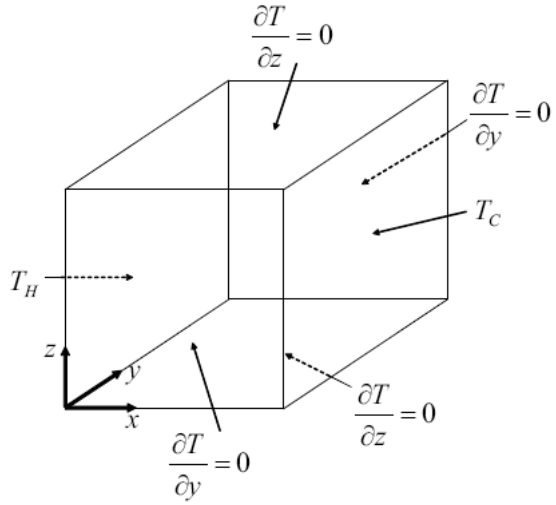

Fig. 3 Schematic geometry for natural convection in a cubic cavity

In the simulation, the Boussinesq approximation is applied to the buoyancy force term.

$$\rho\mathbf{G} = \rho\beta g_0(T - T_m)\mathbf{j} \tag{34}$$

where β is the thermal expansion coefficient, g_0 is the acceleration due to gravity, T_m is the average temperature, and $\mathbf{j}$ is the vertical direction opposite to that of gravity. Therefore the external force F in Eq. (1) can be written as

$$F = 3\mathbf{G}(\mathbf{c} - \mathbf{u})f^{eq} \tag{35}$$

The dynamical similarity depends on two dimensionless parameters; the Prandtl number *Pr* and the Rayleigh number *Ra*,

$$Pr = \frac{\upsilon}{\chi}$$
$$Ra = \frac{g_0\beta\Delta TL^3}{\upsilon\chi} \tag{36}$$

Nusselt number *Nu*, is one of the most important dimensionless numbers in describing the convective transport. Nusselt number at the mid-plane is defined by

$$Nu_{mp} = \int_0^1 \frac{\partial T(y,z)}{\partial x}\partial z \tag{37}$$

In all the simulation, *Pr* is set to be 0.71 and due to the limitation of computer capability, the grid sizes of 101 × 101 is used for the simulation at all

Rayleigh numbers. The convergence criterion for all the tested cases is

$$\max\left|\left(\left(\mathbf{u}^2\right)^{n+1}\right)^{\frac{1}{2}}-\left(\left(\mathbf{u}^2\right)^{n}\right)^{\frac{1}{2}}\right|\le 10^{-7}$$
$$\max\left|T^{n+1}-T^{n}\right|\le 10^{-7} \quad (38)$$

where n is the time step and the calculation is carried out over the entire system.

4 Numerical Results

The comparison among D3Q15, D3Q19 and Navier-Stokes solver [32] are held for Rayleigh numbers 10^3 till 10^5. Among the characteristic numerical values of the flow, the comparisons concern the mean Nusselt number at the mid-plane Nu_{mp}, the maximum value for horizontal and vertical velocity components u_{max} and v_{max} with the positions where they occur (x, y). The comparison is shown in Table 1.

Table 1. Comparison among D3Q15, D3Q19 and Navier-Stokes solvers

	Solver	$Ra=10^3$	$Ra=10^4$	$Ra=10^5$
u_{max}	D3Q15	0.132	0.199	0.166
	D3Q19	0.132	0.200	0.151
	N-S solver	0.131	0.201	0.147
X	D3Q15	0.520	0.529	0.490
	D3Q19	0.480	0.510	0.500
	N-S solver	0.480	0.500	0.500
Y	D3Q15	0.186	0.176	0.138
	D3Q19	0.186	0.182	0.142
	N-S solver	0.200	0.183	0.145
v_{max}	D3Q15	0.132	0.224	0.253
	D3Q19	0.132	0.224	0.248
	N-S solver	0.132	0.225	0.247
X	D3Q15	0.817	0.882	0.892
	D3Q19	0.814	0.883	0.930
	N-S solver	0.883	0.883	0.935
Y	D3Q15	0.500	0.529	0.510
	D3Q19	0.500	0.500	0.500
	N-S solver	0.500	0.500	0.500
Nu_{mp}	D3Q15	1.097	2.301	4.975
	D3Q19	1.096	2.301	4.670
	N-S solver	1.105	2.301	4.646

As can be seen from the table, for the simulation at low Rayleigh number $(Ra=10^3)$, the results obtained were almost the same for D3Q15 and D3Q19 models. However, at high Rayleigh number simulations $(Ra=10^5)$, the results show that the D3Q15 cannot give a satisfactory result when compared with the Navier-Stokes solver for this problem. Furthermore, the D3Q15 is already reported to exhibit the velocity oscillation and low computational mobility [33]. Therefore, the results which will be presented below were obtained from D3Q19 model.

Streamlines and isotherms predicted at mid-plane of the cavity for flows at different Rayleigh numbers are shown in Fig. 4 and Fig. 5.

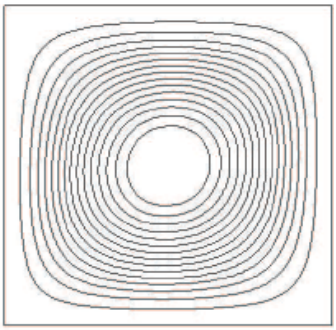

(a) $Ra=10^3$

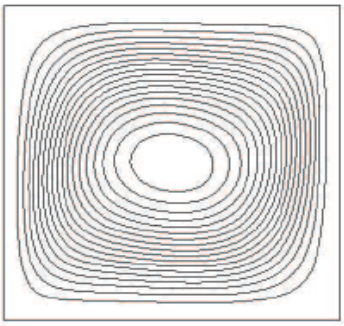

(b) $Ra=10^4$

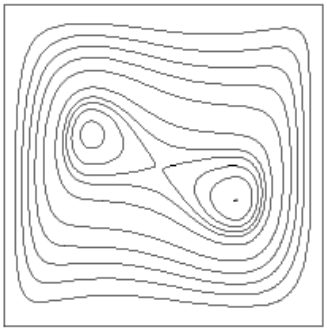

(c) $Ra=10^5$

Fig. 4 Streamline plots for various Rayleigh numbers

At $Ra=10^3$, streamlines are those of a single vortex, with its center in the center of the system. As the Rayliegh number increases $(Ra=10^4)$, the

central streamlines are distorted into an elliptic shape and the effect of convection can be seen in the isotherms. At $Ra=10^5$, the central streamline is elongated and two secondary vortices appear inside it.

At $Ra=10^3$, the isotherms are almost vertically parallel to the wall indicating that conduction is the dominant heat transfer mechanism. As the Rayleigh number is increased to $Ra=10^4$, isotherms start to be horizontally parallel to the wall at the cavity center. This indicates that the heat transfer mechanisms are mixed conduction and convection.

For the simulation at $Ra=10^5$, the isotherms become horizontal at the center of the cavity and vertical only in the thin boundary layer near the cold and hot walls indicating that the dominant of heat transfer mechanism is by convection.

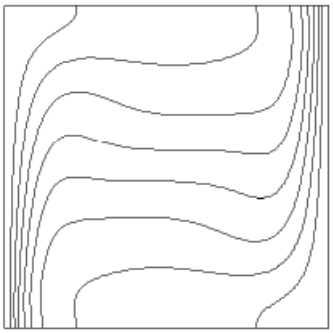

(a) $Ra=10^3$

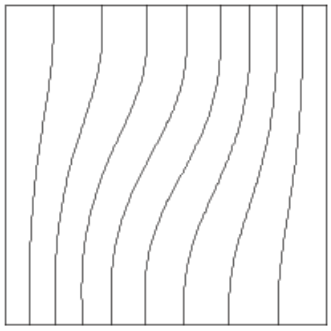

(b) $Ra=10^4$

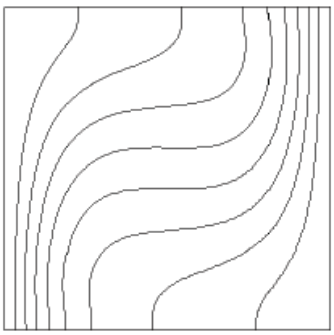

(c) $Ra=10^5$

Fig. 5 Isotherm plots for various Rayleigh numbers

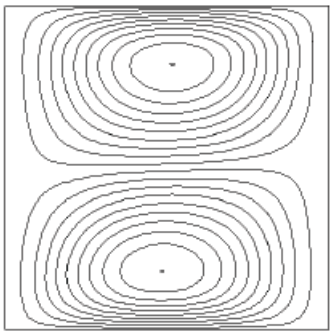

(a) $Ra=10^3$

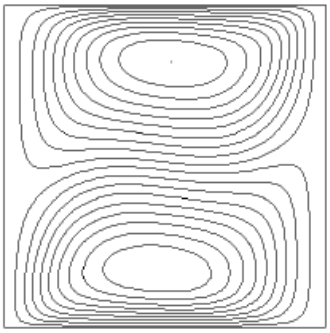

(b) $Ra=10^4$

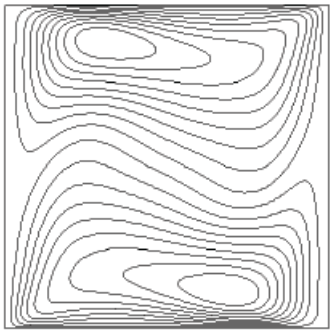

(c) $Ra=10^5$

Fig. 6 Horizontal velocity component for various Rayleigh numbers

The plots of horizontal and vertical components are shown in Figs. 6 and 7. It can be seen from these figures that as the Rayleigh number is increased, the location for maximum velocity moves closer to the wall and their amplitude is also increases. This phenomenon indicates that the fluid motion mainly takes place near the differentially heated walls and the flow in the core cavity becomes quasi-motionless. All of these observations are in good agreement with the results reported in the previous studies [21][23][32][34].

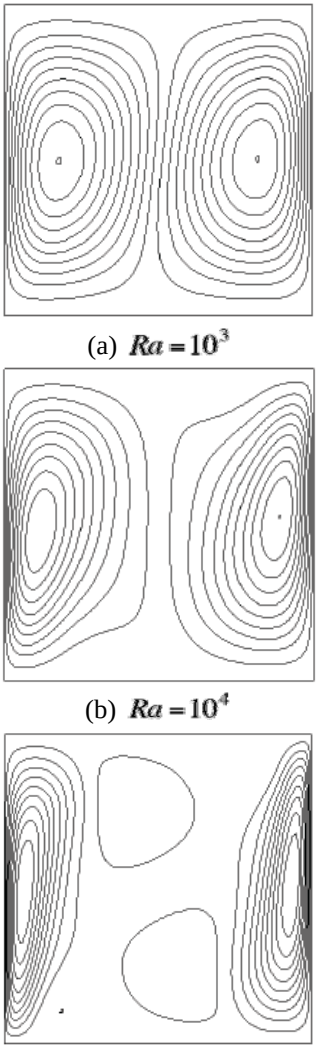

(a) $Ra = 10^3$

(b) $Ra = 10^4$

(c) $Ra = 10^5$

Fig. 7 Vertical velocity component for various Rayleigh numbers

5 Conclusion

In this paper, two types of combinations of three-dimensional thermal lattice Boltzmann formulation were applied and tested on the prediction of natural convection in a cubic cavity. We found that the combination of D3Q15 with D3Q6 exhibit some discrepancies when compared with the Navier-Stokes solution at high Rayleigh numbers simulation for the case investigated and is prone to computational instability.

The results obtained from the combination of D3Q19 and D3Q6 for the same problem correctly predicted the flow features for different Rayliegh numbers and gives excellent agreement with the results of previous studies. These demonstrate the proposed combination in the passive-scalar thermal lattice Boltzmann model is a very efficient numerical method to study flow and heat transfer in a differentially heated cubic enclosure.

Acknowledgement

The authors would like to thank Universiti Teknologi Malaysia and Malaysia government for supporting these research activities.

References:

[1] S. Hou, Q. Zou, S. Chen, G. Doolen and A. C. Cogley, Simulation of Cavity Flow by the Lattice Boltzmann Method, *Journal of Computational Physics*, Vol.118, No.2, 1995, pp. 329-347.

[2] S. Chen and G. Doolen, Lattice Boltzmann Method for Fluid Flows, *Annual Review of Fluid Mechanics*, Vol.30, No.1, 1998, pp. 329-364.

[3] G. Breyiannis and D. Valougeorgis, Lattice Kinetic Simulations in Three-Dimensional Magnetohydrodynamics, *Physical Review E*, Vol.69, No.6, 2004, pp. 065702/1-065702/4.

[4] F. Nathan and H. Richard, Simulating Acoustic Propagation using a Lattice Boltzmann Model of Incompressible Fluid Flow, *WSEAS Transactions on Signal Processing*, Vol.2, No.6, 2006, pp. 876-881.

[5] L. Jonas, B. Chopard, S. Succi and F. Toschi, Numerical Analysis of the Average Flow Field in a Turbulent Lattice Boltzmann Simulation, *Physica A*, Vol.362, No.1, 2006, pp. 6-10.

[6] S. Alapati, S. Kang and Y. K. Suh, 3D Lattice Boltzmann Simulation of Droplet Formation in a Cross-Junction Microchannel, *Proceeding of the 3rd IASME/WSEAS International Conference on Continuum Mechanics*, 2008.

[7] C.S Nor Azwadi and T. Tanahashi, Simplified Thermal Lattice Boltzmann in Incompressible Limit, *International Journal of Modern Physics B*, Vol.20, No.17, 2006, pp. 2437-2449.

[8] I. Halliday and C.M. Care, Steady State Hydrodynamics of Lattice Boltzmann Immiscible Lattice Gas, *Physical Review E*, Vol.53, No.2, 1996, pp. 1602-1612.

[9] C.S. Michael and T.T. Daniel, *Lattice Boltzmann Modeling; An Introduction for Geoscientists and Engineers*, Springer, 2006.

[10] X. Shan and H. Chen, Lattice Boltzmann Model for Simulating Flows with Multiple Phases and Components, *Physical Review E*, Vol.47, No.3, 1993, pp. 1815-1820.

[11] U. Frish, B. Hasslacher and Y. Pomeau, Lattice Gas Automata for the Navier-Stokes Equation,

Physical Review Letters, Vol.56, No.14, 1986, pp. 1505-1508.

[12] G. McNamara and B. Alder, Analysis of Lattice Boltzmann Treatment of Hydrodynamics, *Physica A*, Vol.194, No.1, 1993, pp. 218-228.

[13] X. Shan, Simulation of Rayleigh-Benard Convection using a Lattice Boltzmann Method, *Physical Review E*, Vol.55, No.3, 1997, pp. 2780-2788.

[14] X. He, S. Shan and G. Doolen, A Novel Thermal Model for Lattice Boltzmann Method in Incompressible Limit, *Journal of Computational Physics*, Vol.146, No.1, 1998, pp. 282-300.

[15] H. Chen and C. Teixeira, H-Theorem and Origins of Instability in Thermal Lattice Boltzmann Models, *Computer Physics Communications*, Vol.129, No.1, 2000, pp. 21-31.

[16] P. Lallemand and L.S. Luo, Theory of the Lattice Boltzmann Method: Acoustic and Thermal Properties in Two and Three Dimensions, *Physical Review E*, Vol.68, No.3, 2003, pp. 036706/1-036706/25.

[17] J. Onishi, Y. Chen and H. Ohashi, Lattice Boltzmann Simulation of Natural Convection in a Square Cavity, *JSME International Journal Series B*, Vol.44, No.1, 2001, pp. 45-52.

[18] Y. Peng, C. Shu and Y. T. Chew, Simplified Thermal Lattice Boltzmann for Incompressible Thermal Flow, *Physical Review E*, Vol.68, No.2, 2003, pp. 020671/1-020671/8.

[19] M. Paroncini, F. Corvaro and M.M. Padova, Study and Analysis of the Influence of a Small Heating Source Positioned on the Natural Convective Heat Transfer in a Square Cavity, *WSEAS Transaction on Heat and Mass Transfer*, Vol.1, No.4, 2006, pp. 461-466.

[20] D.V. Davis, Natural Convection of Air in a Square Cavity; A Benchmark Numerical Solution, *International Journal for Numerical Methods in Fluids*, Vol.3, No.3, 1983, pp. 249-264.

[21] Y. Peng, C. Shu and Y.T. Chew, A 3D Incompressible Thermal Lattice Boltzmann Model and its Application to Simulation Natural Convection in a Cubic Cavity, *Journal of Computational Physics*, Vol.193, No.1, 2003, pp. 260-274.

[22] Y.H. Qian, D. Humieres and P. Lallemand, Lattice BGK for Navier-Stokes Equation, *Europhysics Letter*, Vol.17, No.6, 1992, pp. 479-484.

[23] C.S. Nor Azwadi and T. Tanahashi, Three Dimensional Thermal Lattice Boltzmann Simulation of Natural Convection in a Cubic Cavity, *International Journal of Modern Physics B*, Vol.21, No.1, 2007, pp. 87-96.

[24] Z. Guo, B. Shi and C. Zheng, A Coupled Lattice BGK Model for the Boussinesq Equation, *International Journal for Numerical Methods in Fluids*, Vol.39, No.4, 2002, pp. 325-342.

[25] C. Cercignani, *The Boltzmann Equation and its Application in Applied Mathematical Sciences*, Springer, 1988.

[26] S. Harris, *An Introduction to the Theory of the Boltzmann Equation*, Holt, Rinehart and Winston, 1971.

[27] P.L. Bhatnagar, E.P. Gross and M. Krook, A Model for Collision Process in Gasses. 1. Small Amplitude Processes in Charged and Neutral One-Component System, *Physical Review*, Vol.70, No.3, 1954, pp. 511-525.

[28] X. He and L.S. Luo, Lattice Boltzmann Model for the Incompressible Navier-Stokes Equation, *Journal of Statistical Physics*, Vol.88, No.3, 1997, pp. 927-944.

[29] C.S. Nor Azwadi and T. Tanahashi, Simplified Finite Difference Thermal Lattice Boltzmann Method, *International Journal of Modern Physics B*, Vol.22, No.22, 2008, pp. 3865-3876.

[30] H.N. Dixit and V. Babu, Simulation of High Rayleigh Number Natural Convection in a Square Cavity using the Lattice Boltzmann Method, *International Journal of Heat and Mass Transfer*, Vol.49, No.4, 2006, pp. 727-739.

[31] S.H. Sohrab, A Modified Theory of Laminar Flow by Free Convection on a Vertical Hot Surface, *WSEAS Transactions on Biology and Biomedicine*, Vol.2, No.2, 2005, pp. 192-198.

[32] E. Tric, G. Labrosse and M. Betrouni, A First Incursion into the 3D Structure of Natural Convection of Air in a Differentially Heated Cubic Cavity, from Accurate Numerical Solutions, *International Journal of Heat and Mass Transfer*, Vol.43, No.21, 2000, pp. 4043-4056.

[33] R. Mei, W. Shyy, D. Yu and L. S. Luo, Lattice Boltzmann Method for 3-D Flows with Curved Boundary, *Journal of Computational Physics*, Vol.161, No.2, 2000, pp. 680-699.

[34] B. Abdelhadi, G. Hamza, B. Razik and E. Raouache, Natural Convection and Turbulent Instability in Cavity, *WSEAS Transactions on*

Heat and Mass Transfer, Vol.1, No.2, 2006, pp. 179-184.